Journal of The Electrochemical Society, **160** (11) A2234-A2243 (2013)
0013-4651/2013/160(11)/A2234/10/$31.00 © The Electrochemical Society

Ion-Exchangeable Functional Binders and Separator for High Temperature Performance of $Li_{1.1}Mn_{1.86}Mg_{0.04}O_4$ Spinel Electrodes in Lithium Ion Batteries

Seung Hee Woo,[a] Hyung-Woo Lim,[a] Sangbin Jeon,[a] Jonathan J. Travis,[b] Steven M. George,[b,*] Se-Hee Lee,[c,*] Yong Nam Jo,[d] Jun Ho Song,[d] Yoon Seok Jung,[a] Sung You Hong,[a] Nam-Soon Choi,[a,*,z] and Kyu Tae Lee[a,z]

[a]*School of Energy & Chemical Engineering, Ulsan National Institute of Science and Technology (UNIST), Ulju-gun, Ulsan, 689-798, South Korea*
[b]*Department of Chemistry and Biochemistry, University of Colorado at Boulder, Boulder, Colorado 80309-0215, USA*
[c]*Department of Mechanical Engineering, University of Colorado at Boulder, Boulder, Colorado 80309-0215, USA*
[d]*Advanced Batteries Research Center, Korea Electronics Technology Institute, Bundang-gu, Seongnam-si, Gyeonggi-do, 463-816, South Korea*

Since $LiMn_2O_4$ spinel materials are inexpensive, environmentally-friendly, and safe, they are considered a promising cathode candidate for lithium ion batteries in EVs to replace commercialized materials such as $LiCoO_2$, $LiNi_{1/3}Mn_{1/3}Co_{1/3}O_2$ and $LiNi_{0.5}Co_{0.2}Mn_{0.3}O_2$. However, $LiMn_2O_4$ spinel electrodes severely degrade at high temperature due to Mn dissolution. Also, the dissolved Mn^{2+} ions causes self-discharge where reduction of Mn^{2+} ions into Mn metals occurs on a graphite anode surface accompanied by oxidation of lithiated graphite at a charged state, and this results in severe capacity fading at high temperature. In this study, ion-exchangeable binders and a separator having functional groups of sodium carboxylate or sulfonate are, for the first time, examined to solve the Mn dissolution problem of $LiMn_2O_4$ spinel materials at high temperature. Ion exchange between Na^+ ions of the functional groups of the binders and the separator and dissolved Mn^{2+} ions of the $LiMn_2O_4$ electrodes inhibits self-discharge, resulting in improved cycle performance. This result is supported by the IR spectra of the binders, an ICP analysis of the electrolytes, and ex situ XRD patterns of lithiated graphite electrodes.
 [DOI: 10.1149/2.092311jes]

Manuscript submitted August 15, 2013; revised manuscript received September 30, 2013. Published October 12, 2013.

The global major energy source during the past several decades has been fossil fuels, which are finite and harmful to the environment. In efforts to address these problems, electric vehicles operating with clean and sustainable energy systems have been studied, and lithium ion batteries (LIBs) are one of the most promising energy storage devices for electric vehicles (EVs) owing to their high power and energy densities.[1–7] However, the electrochemical performance and safety of LIBs are still not satisfactory for the wide adoption of EVs, and improvement of electrode materials is accordingly demanded. $LiMn_2O_4$ spinel materials are a promising cathode material candidate, because they are less expensive, environmentally-friendly, and safer than commercialized materials including $LiCoO_2$, $LiNi_{1/3}Mn_{1/3}Co_{1/3}O_2$ and $LiNi_{0.5}Co_{0.2}Mn_{0.3}O_2$.[8–11] However, the successful realization of $LiMn_2O_4$ spinel electrodes is quite challenging because $LiMn_2O_4$ spinel electrodes degrade at high temperature,[12–14] resulting in rapid capacity loss. $LiMn_2O_4$ spinel materials have been extensively studied to clarify the mechanisms of capacity fading including Jahn-Teller distortion of Mn^{3+}, formation of oxygen deficient $LiMn_2O_4$ upon cycling, microstrain caused by lattice mismatch between the two distinct cubic phases formed on cycling, and the dissolution of $LiMn_2O_4$ in electrolytes.[15–20] Among them, Mn dissolution is considered to be the predominant cause of capacity fading at high temperature. There are two major factors for Mn dissolution: i) the formation of soluble Mn^{2+} through a disproportionation reaction of $LiMn_2O_4$ ($Mn^{3+} \rightarrow Mn^{2+} + Mn^{4+}$); and ii) acid dissolution by HF ($Li_{1-x}Mn_2O_4 + HF \rightarrow \lambda\text{-}Mn_2O_4 + LiF + Mn^{2+} + H_2O$). Mn dissolution causes a loss of active materials. Moreover, dissolved Mn^{2+} ions diffuse into the graphite anode during cycling; this causes self-discharge where reduction of Mn^{2+} ions into Mn metals occurs on the graphite anode surface accompanied by oxidation of lithiated graphite at a charged state.[21,22] This results in reduced reversible capacity of the graphite anode in a full cell due to irreversible consumption of electrochemically active Li^+ ions. This self-discharge problem is not noticeable in a half-cell configuration because excess amount of Li metal is available from a Li metal counter electrode. However, this problem becomes significant in a full cell with a limited amount of Li ions. Also, reduced manganese species on the anode surface induce accerleration of electrolyte decomposition and increased thickness of the SEI layers results in a rapid increase of polarization.[23] Recently, remarkable improvements in the electrochemical performance of $LiMn_2O_4$ spinel materials have been achieved through the following strategies: i) Substituting Mn with other elements such as Li, Mg, Al, Co, Cr, and Ni effectively suppresses Mn dissolution and Jahn-Teller distortion by increasing the average oxidation state of Mn over 3.5;[24,25] ii) A metal oxide or fluoride coating on the $LiMn_2O_4$ surface acts as a role of HF scavenger via reaction of metal oxides with HF to form MF_x and H_2O;[26–28] iii) Electrolyte additives that neutralize HF acid reduce the amount of Mn dissolution.[29] However, the inherent Mn dissolution problem is still an obstacle to stable cycle performance at high temperature, although previous approaches were successfully employed at room temperature. Herein, we introduce, for the first time, ion-exchangeable binders and a separator that have functional groups of sodium carboxylate or sulfonate as a solution to the Mn dissolution problem. These functional groups of the binders and the separator allow ion exchange between the Na^+ ions of functional groups and dissolved Mn^{2+} ions of $LiMn_2O_4$ electrodes. The ion exchange traps dissolved Mn^{2+} ions to inhibit the reduction of Mn^{2+} on the surface of the lithiated graphite anode, resulting in improved cycle performance at high temperature.

Experimental

Synthesis of a functional separator.— Al_2O_3 ALD films were grown on a porous PE separator at 100°C using a rotary ALD reactor. Detailed ALD reaction sequences have been described in previous reports. Al_2O_3-coated separators were then treated with hydrogen peroxide (30 wt%, Aldrich) for 15 min to introduce OH groups on the surface. Hydroxyl group-terminated separators were immersed in toluene solution of (3-aminopropyl)-triethoxysilane (APTES, 5 wt%) for 8 h, and then washed with toluene and deionized water. Further, APTES-grated separators were reacted with terephthaloyl dichloride in toluene for 2 h at room temperature, and washed with deionized water. Finally, the terephthalic acid-grafted separators were immersed in 0.3 mM sodium hydroxide solution for 8 h at room temperature, and then washed with deionized water.

*Electrochemical Society Active Member.
[z]E-mail: nschoi@unist.ac.kr; ktlee@unist.ac.kr

Characterization.— Infrared spectra were recorded on a Nicolet FT-IR 200 from Thermo Scientific. Powder X-Ray diffraction (XRD) data were collected on a Rigaku D/MAX2500V/PC powder diffractometer using Cu-Kα radiation (λ = 1.5405Å) operated from 2θ = 10 – 80°. SEM samples were examined in a Quanta 200 field-emission scanning electron microscope (FE-SEM) instrument. The atomic composition of the samples was determined by Varian 720-ES inductively coupled plasma (ICP) spectrometry. Surface analysis was examined with XPS (Thermo Fisher).

Electrochemical characterization.— $Li_{1.1}Mn_{1.96}Mg_{0.03}O_4$ (Mitsui Co. Ltd) and graphite (DAG87) materials were received. All binder materials including PVdF, CMC, PSS and AGA were purchased from Aldrich. Samples of electrochemically active materials (80 wt%) were mixed with carbon black (Super P, 10 wt%) and binder (10 wt%). The electrochemical performance was evaluated using 2032 coin cells with a 1.3 M $LiPF_6$ in ethylene carbonate and diethyl carbonate (3:7 v/v) electrolyte solution. Graphite and Li metal were used as an anode for full and half cells, respectively. Galvanostatic experiments were performed at 30°C and 60°C with a current density of 10 mA g^{-1} (ca. 0.1C) in the voltage range of 2.0–4.25 V vs. Li/Li^+. A mole ratio of anode/cathode materials was fixed at 1.1 for the preparation of full cells.

Results and Discussion

Ion-exchangeable binders.— Ion-exchangeable binders that have functional groups of sodium carboxylate or sulfonate were examined as a solution to the Mn dissolution problem. As illustrated in Fig. 1a, we suggest that the functional groups of the binders allow ion exchange between the Na^+ ions of functional groups and dissolved Mn^{2+} ions of $LiMn_2O_4$ electrodes, resulting in traping dissolved Mn^{2+} ions to inhibit the reduction of Mn^{2+} on the surface of the lithiated graphite anode. In this study, sodium carboxymethyl cellulose (CMC), poly(sodium 4-styrene sulfonate) (PSS), and sodium alginate (AGA) were utilized as functional binders (see chemical structures in Fig. 1b). The cycle performance of $Li_{1.1}Mn_{1.86}Mg_{0.04}O_4$ spinel at 60°C was improved due to the ion exchange functionality of the binders. This result was supported by the IR spectra of the binders, an ICP analysis of the electrolytes, and ex situ XRD patterns of lithiated graphite electrodes.

To clearly show the role of ion exchange in cycle performance at high temperature, commercialized $Li_{1.1}Mn_{1.86}Mg_{0.04}O_4$ spinel materials (Mitsui Co. Ltd) providing state-of-the-art performance were utilized to evaluate the electrochemical performance of the functional binders. A XRD pattern and SEM image of $Li_{1.1}Mn_{1.96}Mg_{0.03}O_4$ spinel are presented in Figs. 2a-2b. $Li_{1.1}Mn_{1.86}Mg_{0.04}O_4$ spinel showed very stable cycle performance with a reversible capacity of ca. 100 mA h g^{-1} at 30°C and even at 60°C, when examined using a half cell with a Li metal anode (Fig. 3a). The corresponding voltage profiles are presented in Fig. 4. The electrode exhibited 96.3% and 87.4% capacity retention after 30 cycles at 30°C and 60°C, respectively. This indicates that the main cause of capacity fading of manganese spinels is not related to the positive electrode side, including mass loss of active materials. However, full cells comprised of a $Li_{1.1}Mn_{1.86}Mg_{0.04}O_4$ spinel cathode and a graphite anode showed different behavior from half cells. A XRD pattern and SEM image of graphite powders are presented in Figs. 2c-2d. As shown in Fig. 3b, the full cells showed stable cycle performance with a reversible capacity of ca. 90 mA h g^{-1} at 30°C, but exhibited severe capacity fading at 60°C. Some amount of electrochemically active Li in $LiMn_2O_4$ was consumed to form solid electrolyte interphase on anode during the first charging process, and this results in delivering the lower reversible capacities of full cells (ca. 90 mA h g^{-1} at 30°C) than those of half cells (ca. 105 mA h g^{-1} at 30°C). The corresponding voltage profiles are presented in Fig. 5. For the full cells, all electrodes were prepared using a conventional PVdF binder. As reported previously, this capacity fading at high temperature is attributed to the dissolved manganese ions, which cause self-discharge of lithiated electrodes. Therefore, ion-exchangeable polymers with functional groups of sodium carboxylate and sulfonate including CMC, AGA, and PSS were examined as binders for graphite anodes to alleviate the self-discharge that the dissolved manganese ions reduce on the surface of lithiated graphite anodes, as shown in the schematic diagram (Fig. 1a). The concept of ion exchangeable binders is mimetic of a cation exchange resin for water softening. Cation exchange resins are used to replace the magnesium or calcium ions found in hard water with sodium ions, and the ion exchange progresses until reaching equilibrium with much lower concentrations of magnesium or calcium ions in solution than the initial concentrations. The ion exchange relies on coulombic interaction between the negative charge immobilized on the resin (COO^- or SO_3^-) and the opposite positive charge of samples such as Mg^{2+} or Ca^{2+}. According to this principle, the trapping of Mn^{2+} ions by ion-exchangeable binders takes place with simultaneous release of Na^+ ions due to the stronger coulombic attraction between divalent Mn^{2+} ions and the negative charge of anionic functional groups of binders compared to monovalent Na^+. This process reaches equilibrium with a decreased concentration of manganese ions in electrolytes, resulting in alleviation of self-discharge by dissolved Mn^{2+} ions.

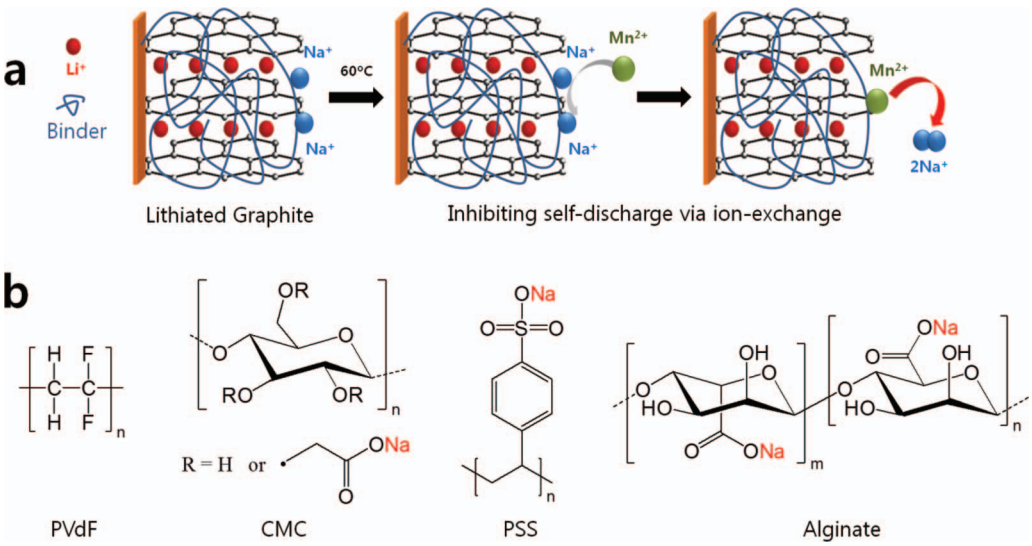

Figure 1. (a) Schematic diagram for the principle of ion-exchangeable binders. (b) Chemical structures of various binders.

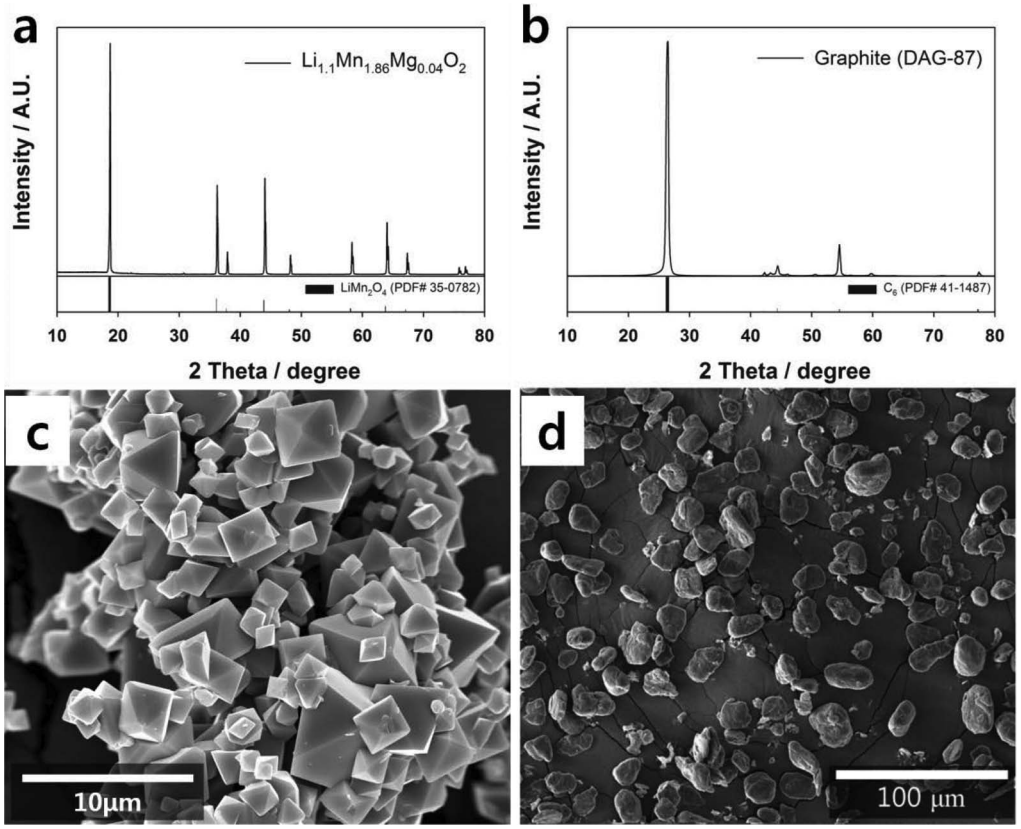

Figure 2. XRD patterns of (a) $Li_{1.1}Mn_{1.86}Mg_{0.04}O_2$ and (b) graphite. SEM images of (c) $Li_{1.1}Mn_{1.86}Mg_{0.04}O_2$ and (d) graphite.

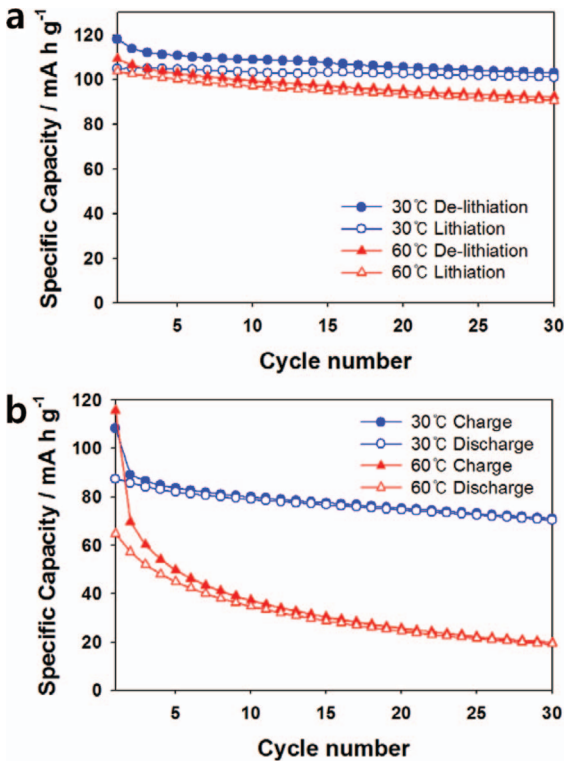

Figure 3. (a) Cycle performance of a $Li_{1.1}Mn_{1.86}Mg_{0.04}O_2$ cathode at 30°C and 60°C using a half cell with a Li metal anode. (b) Cycle performance of a full cell comprised of a $Li_{1.1}Mn_{1.86}Mg_{0.04}O_2$ cathode and a graphite anode prepared with PVdF binder at 30°C and 60°C.

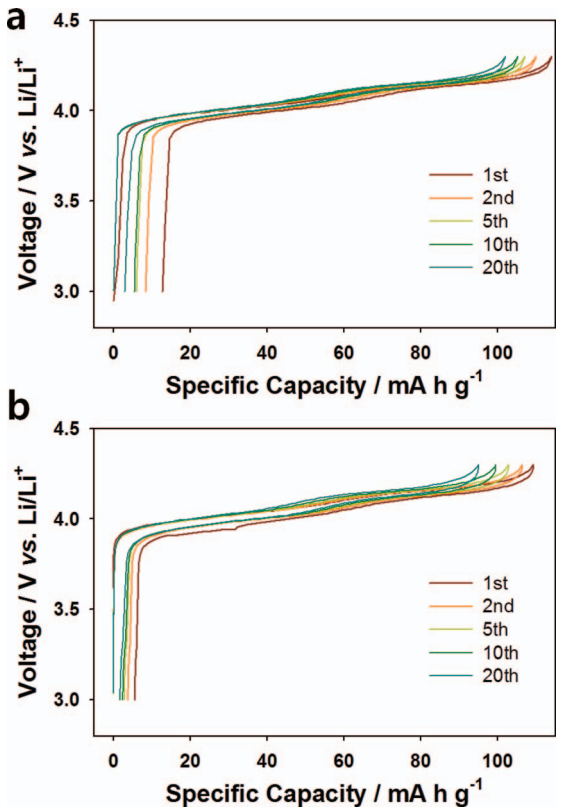

Figure 4. Voltage profiles of a $Li_{1.1}Mn_{1.86}Mg_{0.04}O_2$ cathode using a half cell with a Li metal anode at (a) 30°C and (b) 60°C.

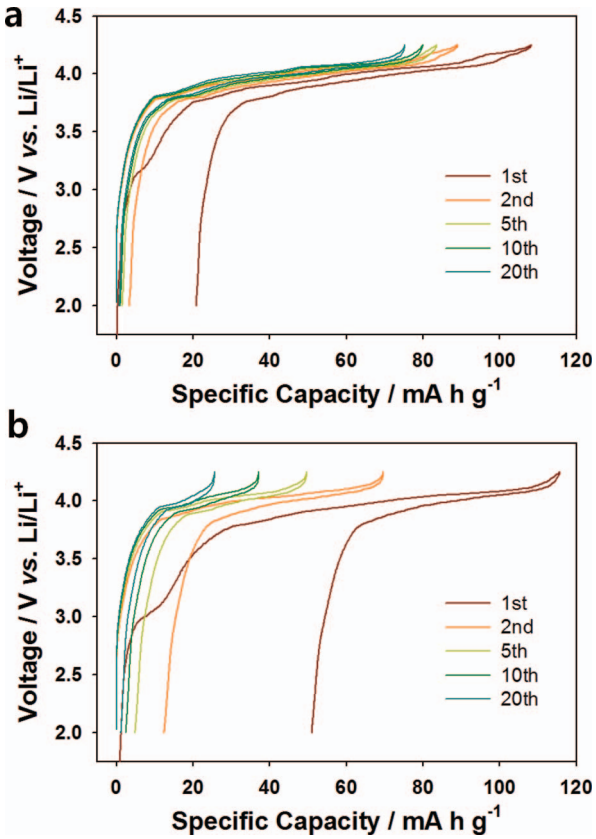

Figure 5. Voltage profiles of a full cell comprised of a $Li_{1.1}Mn_{1.86}Mg_{0.04}O_2$ cathode and a graphite anode prepared with PVdF binder at (a) 30°C and (b) 60°C.

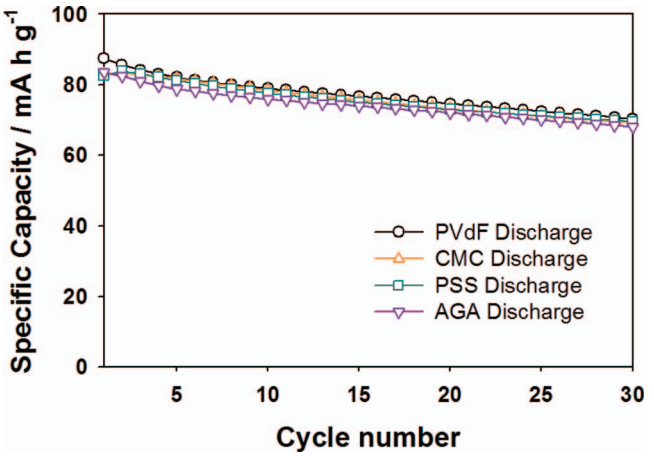

Figure 7. Cycle performance of full cells comprised of a $Li_{1.1}Mn_{1.86}Mg_{0.04}O_2$ cathode prepared with PVdF and a graphite anode prepared with various binders at 30°C.

Figures 6 and 7 show the voltage profiles of full cells at 30°C and the corresponding cycle performance, respectively. All binders including PVdF and ion-exchangeable binders showed similarly stable cycle performance with a reversible capacity of ca. 80–90 mA h g^{-1}, and this is ascribed to the manganese dissolution not being severe during cycling at 30°C. However, at 60°C, all ion exchangeable binders exhibited better cycle performance than PVdF due to the ion exchange effect of the binders, as shown in Figs. 8. The reversible capacity of full cells at 60°C was smaller than that at 30°C. This is attributed to that the more amount of electrochemically active Li in $LiMn_2O_4$ electrodes were irreversibly consumed at 60°C to form SEI on the surface of graphite anodes, as shown in the poorer coulombic efficiencies of full

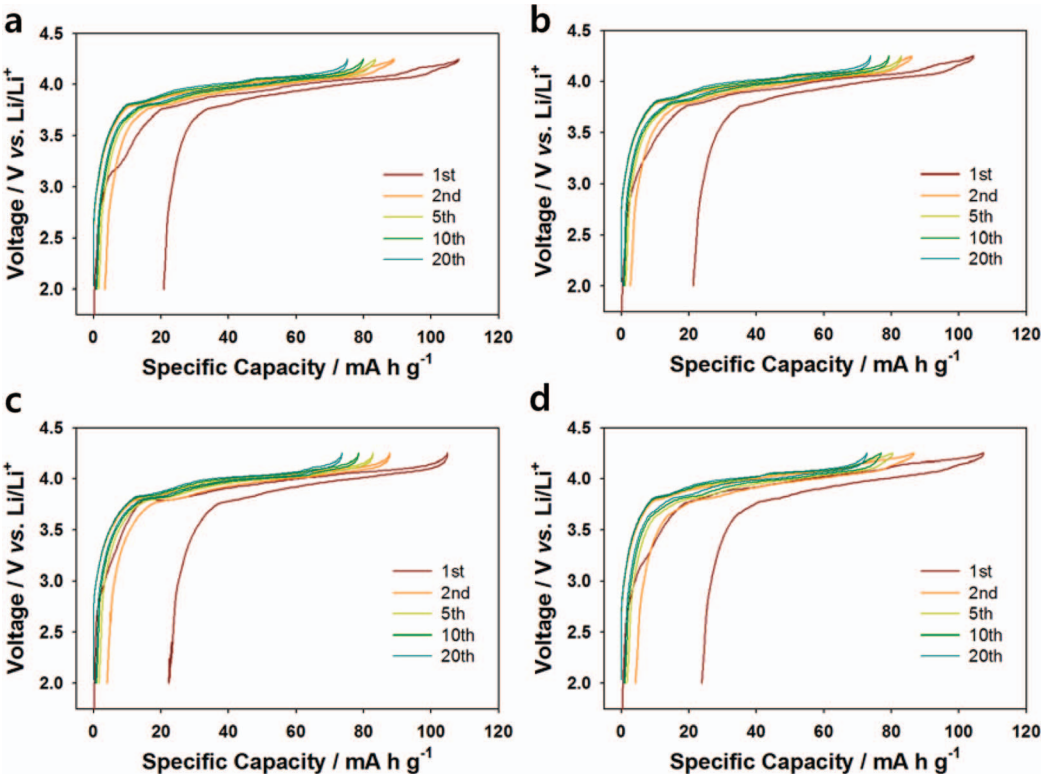

Figure 6. Voltage profiles of full cells comprised of a $Li_{1.1}Mn_{1.86}Mg_{0.04}O_2$ cathode prepared with PVdF and a graphite anode prepared with (a) PVdF, (b) CMC, (c) PSS, and (d) AGA binders at 30°C.

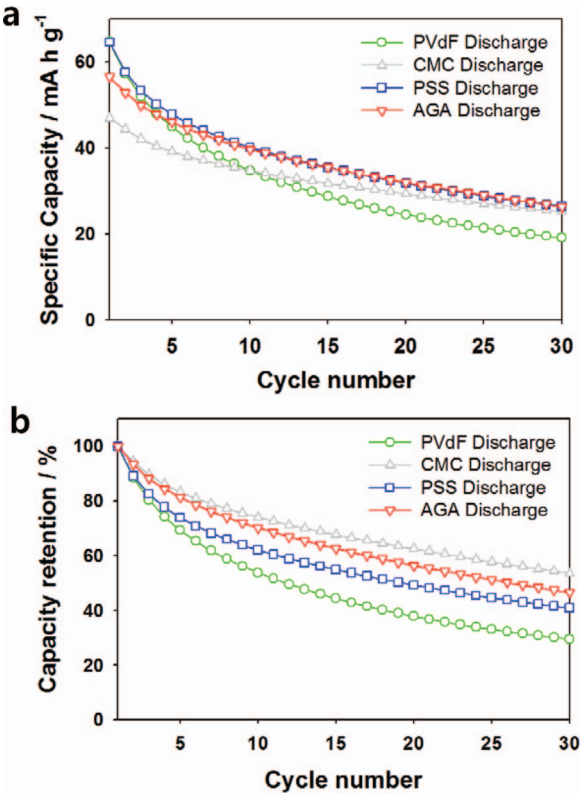

Figure 8. (a) Cycle performance and (b) normalized capacity retention of full cells comprised of a $Li_{1.1}Mn_{1.86}Mg_{0.04}O_2$ cathode prepared with PVdF and a graphite anode prepared with various binders at 60°C.

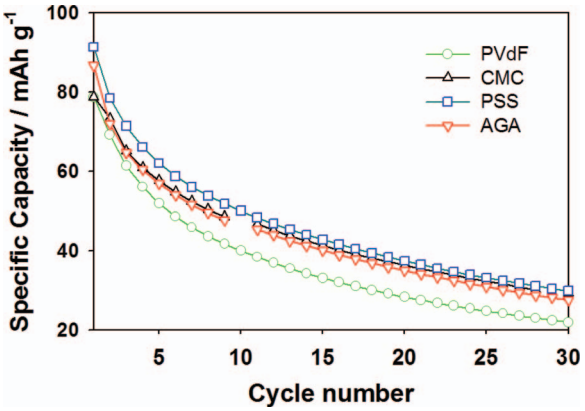

Figure 10. Cycle performance of full cells comprised of a $Li_{1.1}Mn_{1.86}Mg_{0.04}O_2$ cathode prepared with PVdF and a graphite anode prepared with various binders at 60°C after pre-cycling at 30°C.

cells at 60°C than at 30°C (Fig. 9). This is further supported by Figs. 10 and 11. The electrochemical performance of full cells with precycling at 30°C was compared. When SEI was formed at 30°C before cycling, the reversible capacities at 60°C increased to ca. 80–90 mA h g^{-1} compared to without precycling. This is ascribed by that the consumed amount of electrochemically active Li in $LiMn_2O_4$ electrodes for SEI formation was alleviated due to precycling at 30°C, as shown in the enhanced coulombic efficiencies of Fig. 11. Also, Figure 10 showsthe cycle performance of full cells at 60°C with precycling at 30°C. They showed the same behavior of cycle performance compared to the case of without precycling, indicating the ion exchange is effective regardless of the amount of SEI formation.

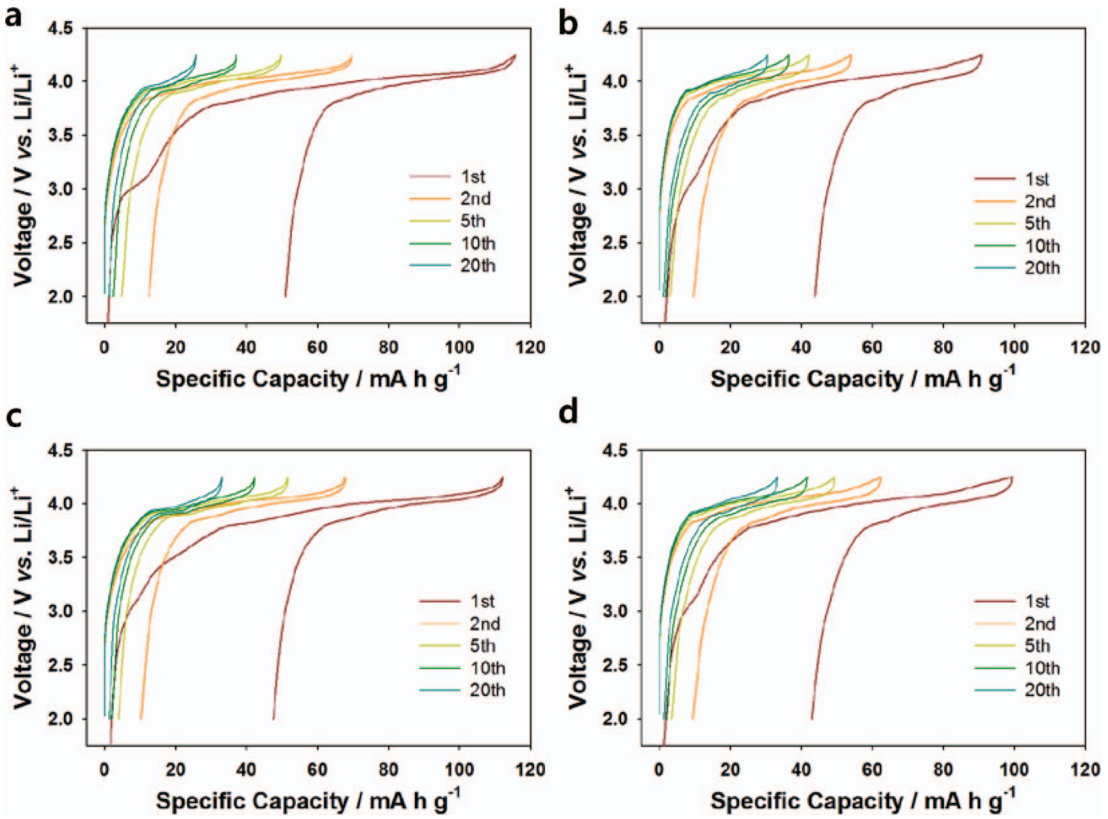

Figure 9. Voltage profiles of full cells comprised of a $Li_{1.1}Mn_{1.86}Mg_{0.04}O_2$ cathode prepared with PVdF and a graphite anode prepared with (a) PVdF, (b) CMC, (c) PSS, and (d) AGA binders at 60°C.

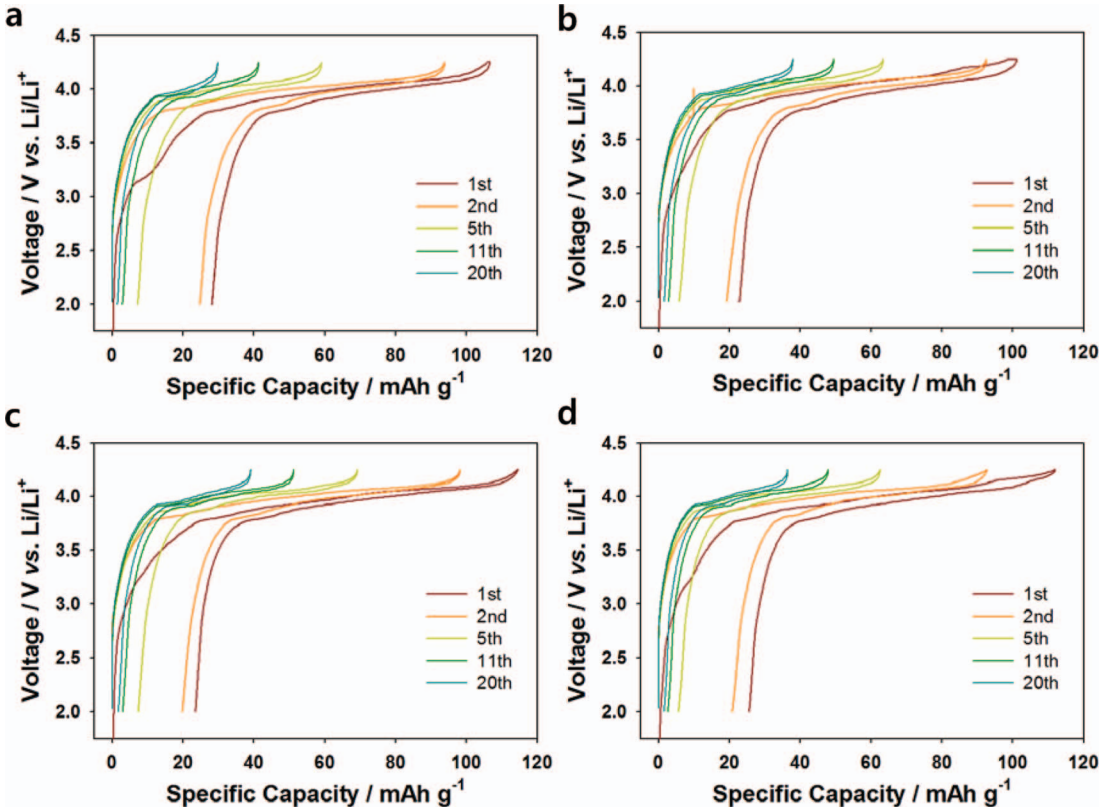

Figure 11. Voltage profiles of full cells comprised of a $Li_{1.1}Mn_{1.86}Mg_{0.04}O_2$ cathode prepared with PVdF and a graphite anode prepared with (a) PVdF, (b) CMC, (c) PSS, and (d) AGA binders at 60°C after pre-cycling at 30°C.

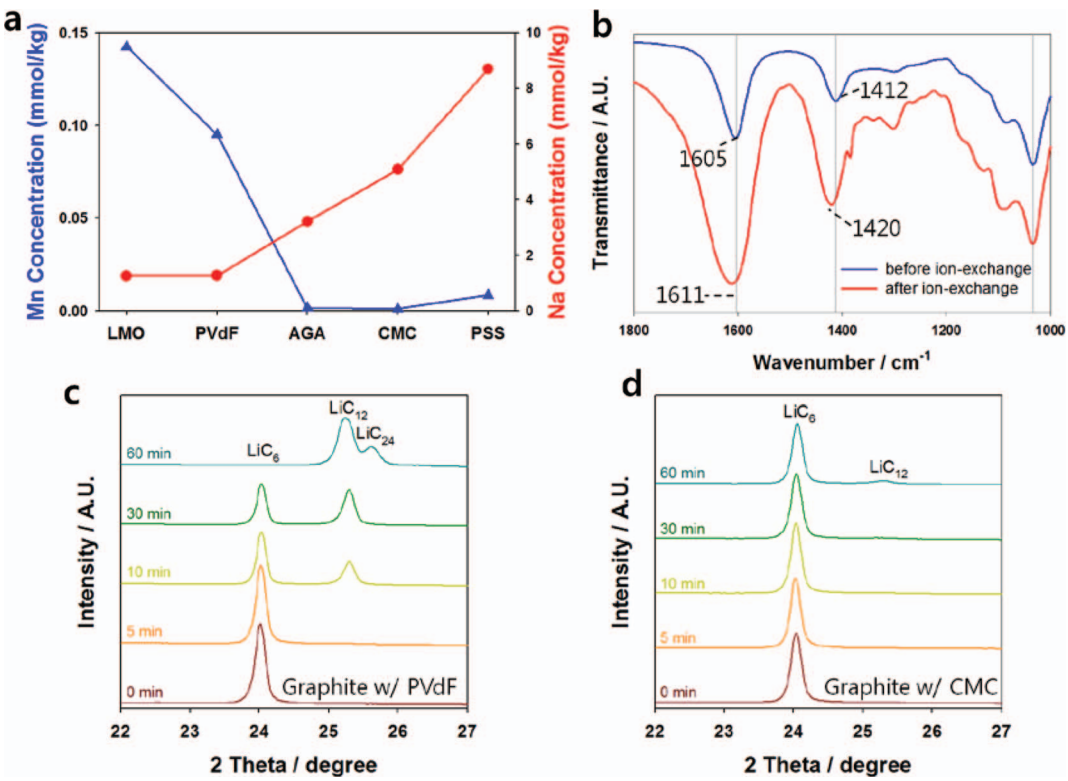

Figure 12. (a) Change of Mn and Na concentrations after soaking of the various binders in the manganese-dissolved electrolyte for 1 week. (b) IR spectra of the alginic acid binder obtained before and after storage in the manganese-dissolved electrolyte. Variation of XRD peaks related to the LiC_6 phase of the fully lithiated graphite electrode prepared with (c) PVdF and (d) CMC binders due to self-discharge with and without ion exchange.

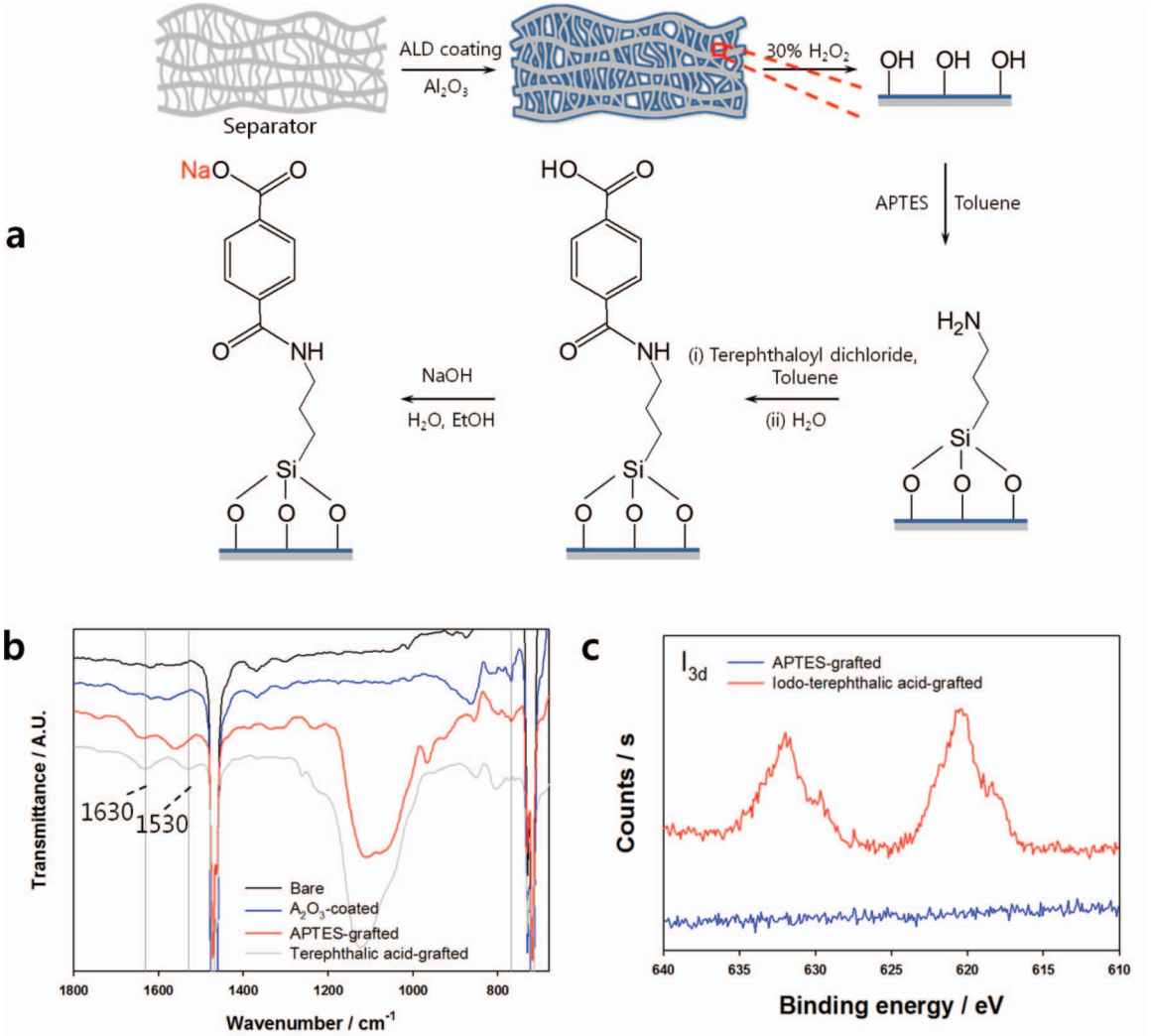

Figure 13. (a) Schematic diagram for the synthesis of an ion-exchangeable separator. (b) IR spectra of various surface-treated separators. (c) XPS spectra of APTES-grafted and iodo-terephthalic acid-grafted separators.

The occurrence of ion exchange between dissolved Mn^{2+} ions in electrolytes and Na^+ ions of binders was supported by three experiments. First, the change of the Na^+ and Mn^{2+} concentrations in the electrolytes was respectively measured via inductively coupled plasma mass spectrometry (ICP-MS) before and after ion exchange occurred. A Mn-dissolved electrolyte solution was prepared via storage of $Li_{1.1}Mn_{1.86}Mg_{0.04}O_4$ powders in a 1.3 M $LiPF_6$-dissolved EC:DEC (3:7, v/v) solution at 60°C for 1 week, and then the remaining $Li_{1.1}Mn_{1.86}Mg_{0.04}O_4$ powders were removed through filtration. A considerable amount of manganese ions was dissolved in the electrolyte at 60°C, and the Mn^{2+} concentration of the resulting electrolyte solution was 0.143 mmol/kg after storage. Powders of each binder were then soaked in the obtained manganese-dissolved electrolyte solution with the same weight ratio of binder/solution (300 mg/5 mL). After soaking for 1 week, each binder powder was removed again through filtration, and the changes of the Na^+ and Mn^{2+} concentrations of the resulting solutions were measured. As shown in Fig. 12a, while the Mn^{2+} concentration of the electrolyte solution slightly decreased to 0.095 mmol/kg in the case of the PVdF binder, for the other ion-exchangeable binders, a negligible amount of Mn^{2+} (0.002, 0.001, and 0.008 mmol/kg for AGA, CMC, and PSS, respectively) remained in the electrolytes and the concentration of Na^+ increased substantially after storage of binders. This implies that Mn^{2+} was bound to the functional groups of the binders due to the ion-exchange effect. Also, after the storage of ion-exchangeable binders, the Na^+ concentration was much higher than the expected value from ion exchange with Mn^{2+} in the electrolytes. This is attributed to ion exchange between Li^+ of $LiPF_6$ salts and Na^+ of the binders. The occurrence of ion exchange was further supported by the IR spectra of the alginate binder obtained before and after storage in the manganese-dissolved electrolyte (Fig. 12b). The bands at 1412 cm^{-1} and 1605 cm^{-1} were assigned to symmetric and asymmetric stretching of sodium carboxylate in the alginate binder. The ion-exchanged alginate binder with Mn^{2+} presented blue-shifted signals compared to the carboxylate peaks of the bare alginate binder. Finally, variation of the XRD patterns of fully lithiated graphite electrodes was observed due to self-discharge with and without ion exchange. Graphite electrodes were first fully lithiated to form a LiC_6 phase using half-cells when the redox potential reached 0 V vs. Li/Li^+. The cells were then disassembled and the fully lithiated graphite electrodes were soaked in the manganese-dissolved electrolyte solutions. After various soaking durations from 0 to 60 min, the XRD patterns of the lithiated graphite electrodes were obtained. As shown in Fig. 12c, after 10 min, the XRD peaks related to the LiC_6 phase of the lithiated graphite electrode prepared with the PVdF binder began to diminish with the appearance of a secondary phase of LiC_{12}. A mixture of LiC_{12} and LiC_{24} phases were subsequently observed after 60 min, accompanying the entire disappearance of the LiC_6 phase. This is attributed to the reduction of dissolved Mn^{2+} ions into the Mn metal through oxidation of the lithiated graphite. However, in the case of the fully lithiated graphite electrodes prepared with the

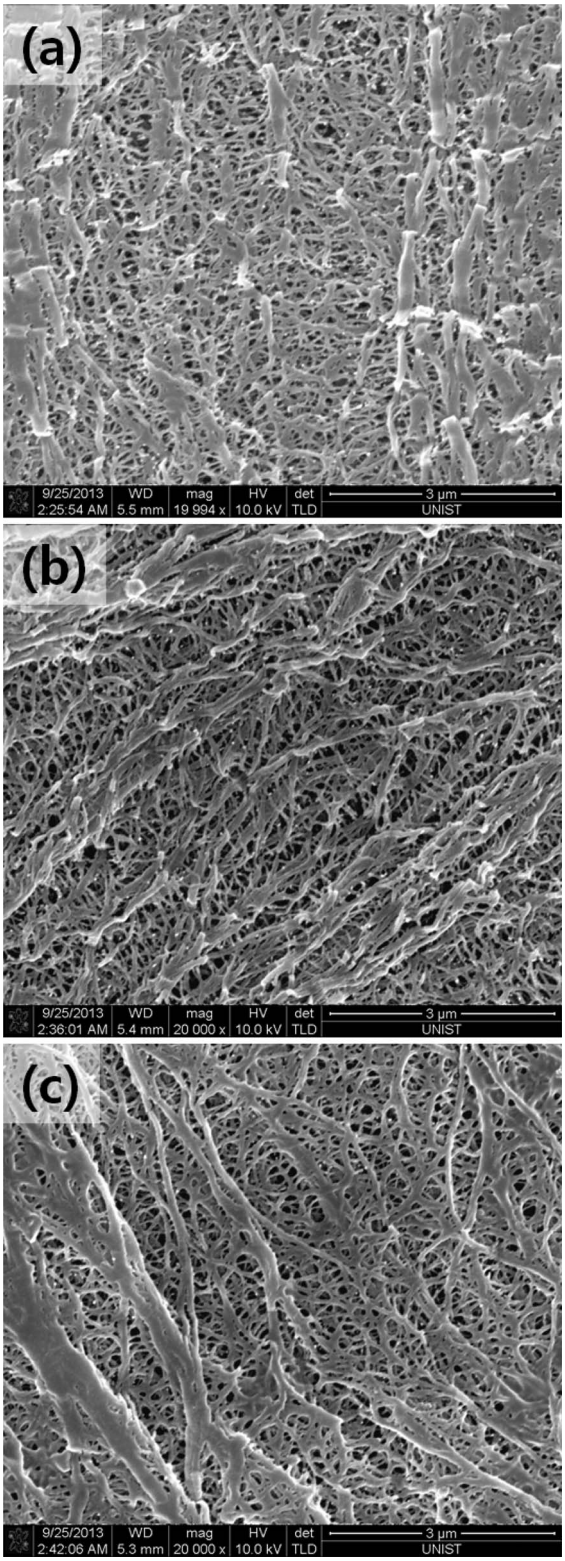

Figure 14. SEM images of (a) bare, (b) Al_2O_3-coated, and (c) Na terephthalate-grafted PE separators.

CMC binder, a negligible amount of LiC_{12} phase was observed even after 60 min (Fig. 12d), and this is ascribed to most of the dissolved Mn^{2+} ions having been preferentially exchanged with Na^+ ions of binders. Binding of Mn^{2+} ions to carboxylate groups of the binders alleviates the reduction of Mn^{2+} ions on lithiated graphites, resulting in improved of cycle performance.

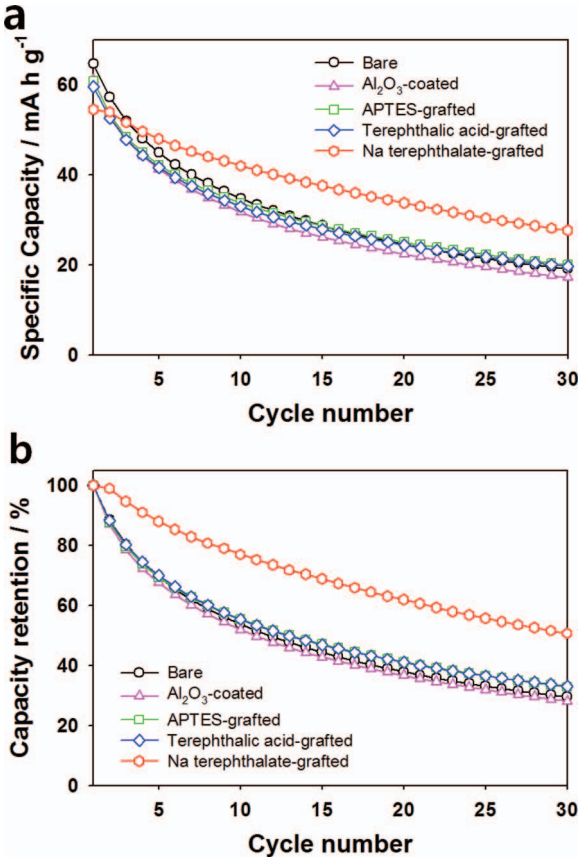

Figure 15. (a) Cycle performance and (b) normalized capacity retention of full cells comprised of a $Li_{1.1}Mn_{1.86}Mg_{0.04}O_2$ cathode, a graphite anode, and various separators at 60°C.

Ion-exchangeable separator.— In addition, an ion exchangeable separator having a functional group of sodium carboxylate was synthesized to improve the cycle performance of the $Li_{1.1}Mn_{1.86}Mg_{0.04}O_4$ electrode, as shown in the schematic diagram (Fig. 13a).[30,31] First, Al_2O_3 was homogenously coated on conventional polyethylene (PE) separators via atomic layer deposition (ALD), as previously reported.[32,33] The Al_2O_3 surface was hydroxylated with H_2O_2, and then 3-aminopropyl triethoxysilane (APTES) was grafted onto the hydroxylated Al_2O_3 surface.[34] The terephthaloyl dichloride was further coupled with the amine group of grafted APTES through the formation of an amide group, followed by rinsing with deionized water. Finally, carboxylic acid groups of the functionalized separator were changed into sodium carboxylates by treatment with NaOH.[35] This synthesis was supported by IR spectra of the surface-functionalized separators, as shown in Fig. 13b. Broad IR bands near 1000∼1200 cm^{-1} were observed after treatment with APTES, indicating Si-O-Si stretching of APTES. After conjugation of terephthalic acid motif with APTES, small peaks at 1530 cm^{-1} and 1630 cm^{-1} were observable and assigned to the aromatic ring of terephthalic acid and an amide group, respectively. In order to clearly show that the terephthalic acid motif is grafted onto the separators, the activated 2-iodoterephthaloyl dichloride was reacted with the APTES-functionalized separator, because iodine is one of the most sensitive elements detectable by XPS. Figure 13c shows that two peaks were observed at 621 and 632 eV in the I 3d XPS binding energy region after grafting 2-iodo-terephthalic acid motif, indicating that terephthalic acid is grafted on the APTES-functionalized Al_2O_3 surface. Figure 14 shows SEM images of bare, Al_2O_3-coated, and Na terephthalate-grafted PE separators, and they have similar pore size and morphologies without pore blocking, indicating that separators were homogenously coated by thin layers of Al_2O_3 and Na terephthalate. Figures 15 and 16 show

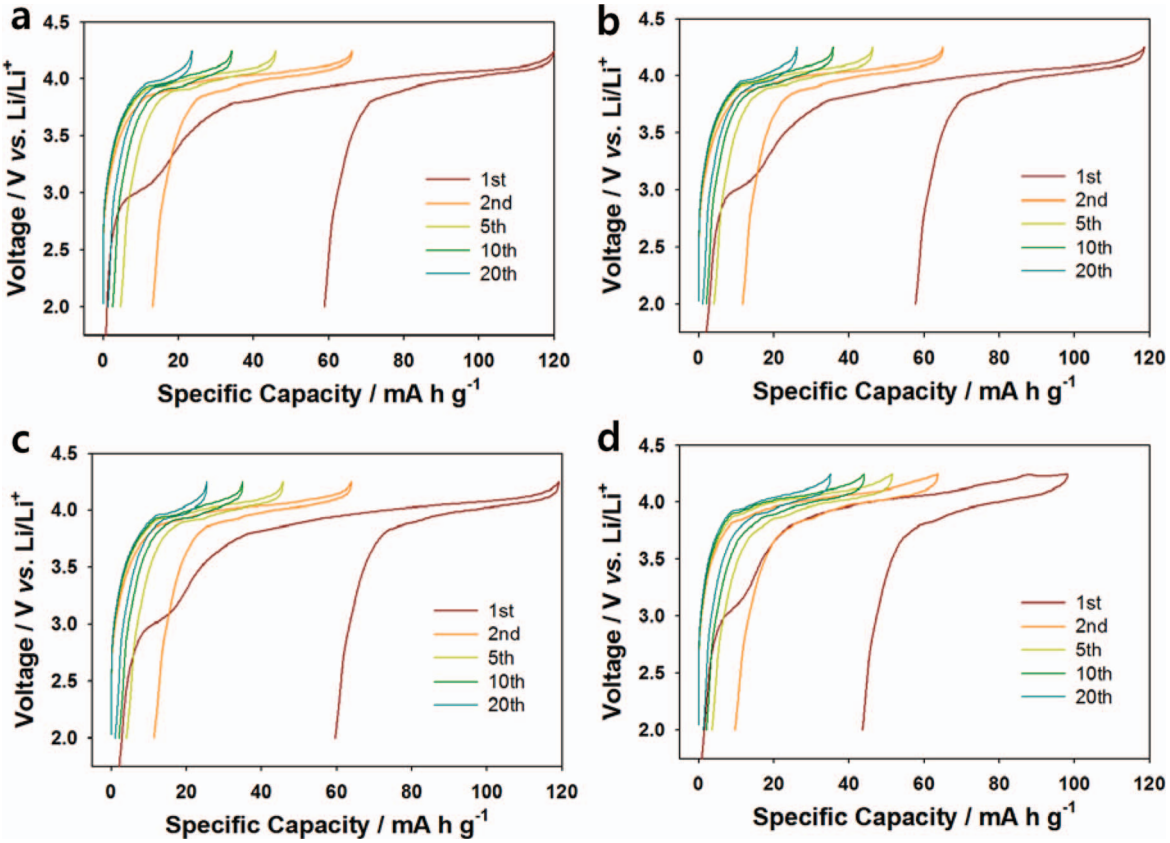

Figure 16. Voltage profiles at 60°C of full cells comprised of a $Li_{1.1}Mn_{1.86}Mg_{0.04}O_2$ cathode, a graphite anode, and (a) Al_2O_3-coated, (b) APTES-grafted, (c) terephthalic acid-grafted, or (d) ion-exchangeable terephthalate-grafted separator.

the cycle performance at 60°C of full cells prepared with various surface-treated separators and their corresponding voltage profiles, respectively. Full cells were comprised of a $Li_{1.1}Mn_{1.86}Mg_{0.04}O_4$ spinel cathode and a graphite anode, and both electrodes were prepared with PVdF binders. It is notable that only the ion exchangeable separator functionalized with terephthalic acid sodium salt improved cycle performance at 60°C, and the other separators including Al_2O_3-coated, APTES-grafted, and terephthalic acid-grafted separators showed similar cycle performance to the bare PE separator. This indicates that the improved cycle performance is attributed to the ion exchange between dissolved Mn^{2+} ions and Na^+ ions of the functionalized separator with sodium terephtalate, as shown in the schematic diagram (Fig. 17).

Conclusions

In conclusion, ion-exchangeable binders and a separator having functional groups of sodium carboxylate or sulfonate were, for the first time, synthesized and examined to improve the high temperature cycle performance of $Li_{1.1}Mn_{1.86}Mg_{0.04}O_4$ spinel cathode materials. Ion exchange occurs between the Na^+ ions of the functional groups of the binders and the separator and the dissolved Mn^{2+} ions of the $LiMn_2O_4$ electrodes. This trapping of dissolved Mn^{2+} ions inhibits self-discharge such as the reduction of Mn^{2+} on the surface of the lithiated graphite anode, resulting in improved cycle performance. In this report, sodium carboxymethyl cellulose (CMC), poly(sodium 4-styrene sulfonate) (PSS), and sodium alginate (AGA) were utilized as functional binders, and a surface-functionalized separator with sodium terephthalate was synthesized as an ion exchangeable separator. Using these functional binders and separator, the cycle performance of $Li_{1.1}Mn_{1.86}Mg_{0.04}O_4$ spinel at 60°C was highly improved due to the ion exchange effect. The ion exchange phenomena were supported by the IR spectra of the binders, an ICP analysis of the electrolytes, and ex situ XRD patterns of lithiated graphite electrodes. It is expected that these functional binders and separator can be extended to other manganese-based cathode materials including $LiNi_{0.5}Mn_{1.5}O_4$ and Li_2MnO_3-$LiMO_2$.

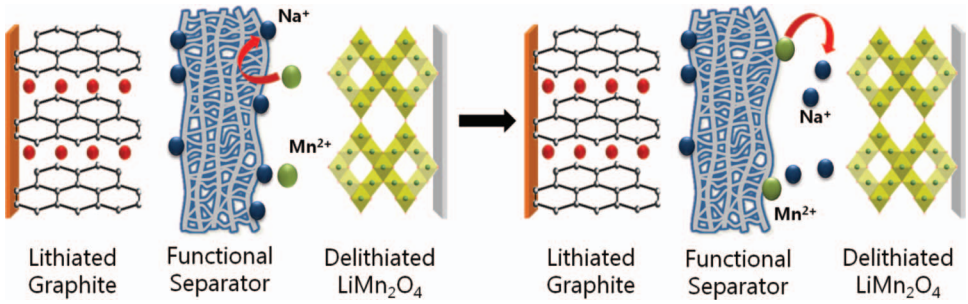

Figure 17. Schematic diagram for the principle of an ion-exchangeable separator.

Acknowledgment

This research was supported by the MSIP (Ministry of Science, ICT&Future Planning), Korea, under the C-ITRC(Convergence Information Technology Research Center) support program (NIPA-2013-H0301-13-1009) supervised by the NIPA(National IT Industry Promotion Agency)**,** by the National Research Foundation of Korea (NRF) grant funded by the Korea Government (MEST) (No. 2010-0019408), and by the Ministry of Knowledge Economy(MKE), Korea Institute for Advancement of Technology(KIAT) through the Inter-ER Cooperation Projects. This work was also partly supported by the IT R&D program of MKE/KEIT (KI001810039182, development of 5 V cathode material which capacity is 125 mA g^{-1} and high voltage electrolyte which decomposition is over 5 V for lithium secondary battery).

References

1. M. Armand and J. M. Tarascon, *Nature*, **451**(7179), 652 (2008).
2. M. M. Thackeray, C. Wolverton, and E. D. Isaacs, *Energy & Environmental Science*, **5**(7), 7854 (2012).
3. J. Arai, T. Yamaki, S. Yamauchi, T. Yuasa, T. Maeshima, T. Sakai, M. Koseki, and T. Horiba, *Journal of Power Sources*, **146**(1–2), 788 (2005).
4. Z. H. Chen, D. J. Lee, Y. K. Sun, and K. Amine, *Mrs Bulletin*, **36**(7), 498 (2011).
5. N. S. Choi, Z. H. Chen, S. A. Freunberger, X. L. Ji, Y. K. Sun, K. Amine, G. Yushin, L. F. Nazar, J. Cho, and P. G. Bruce, *Angewandte Chemie-International Edition*, **51**(40), 9994 (2012).
6. J. Kim, H. Kim, I. Park, Y. U. Park, J. K. Yoo, K. Y. Park, S. Lee, and K. Kang, *Energy & Environmental Science*, **6**(3), 830 (2013).
7. J. A. Choi, S. H. Kim, and D. W. Kim, *Journal of Power Sources*, **195**(18), 6192 (2010).
8. B. L. Ellis, K. T. Lee, and L. F. Nazar, *Chemistry of Materials*, **22**(3), 691 (2010).
9. M. M. Thackeray, *Journal of the American Ceramic Society*, **82**(12), 3347 (1999).
10. G. Amatucci and J. M. Tarascon, *Journal of the Electrochemical Society*, **149**(12), K31 (2002).
11. E. Hosono, T. Kudo, I. Honma, H. Matsuda, and H. S. Zhou, *Nano Letters*, **9**(3), 1045 (2009).
12. R. J. Gummow, A. Dekock, and M. M. Thackeray, *Solid State Ionics*, **69**(1), 59 (1994).
13. N. S. Choi, J. T. Yeon, Y. W. Lee, J. G. Han, K. T. Lee, and S. S. Kim, *Solid State Ionics*, **219**, 41 (2012).
14. G. G. Amatucci, N. Pereira, T. Zheng, and J. M. Tarascon, *Journal of the Electrochemical Society*, **148**(2), A171 (2001).
15. D. H. Jang and S. M. Oh, *Journal of the Electrochemical Society*, **144**(10), 3342 (1997).
16. J. Cho and M. M. Thackeray, *Journal of the Electrochemical Society*, **146**(10), 3577 (1999).
17. J. M. Tarascon, W. R. McKinnon, F. Coowar, T. N. Bowmer, G. Amatucci, and D. Guyomard, *Journal of the Electrochemical Society*, **141**(6), 1421 (1994).
18. M. Hirayama, H. Ido, K. Kim, W. Cho, K. Tamura, J. Mizuki, and R. Kanno, *Journal of the American Chemical Society*, **132**(43), 15268 (2010).
19. D. Kim, S. Park, O. B. Chae, J. H. Ryu, Y. U. Kim, R. Z. Yin, and S. M. Oh, *Journal of the Electrochemical Society*, **159**(3), A193 (2012).
20. Y. J. Shin and A. Manthiram, *Electrochemical and Solid State Letters*, **5**(3), A55 (2002).
21. A. Blyr, C. Sigala, G. Amatucci, D. Guyomard, Y. Chabre, and J. M. Tarascon, *Journal of the Electrochemical Society*, **145**(1), 194 (1998).
22. S. Komaba, N. Kumagai, and Y. Kataoka, *Electrochimica Acta*, **47**(8), 1229 (2002).
23. Z. H. Chen and K. Amine, *Journal of the Electrochemical Society*, **153**(2), A316 (2006).
24. Y. K. Sun, C. S. Yoon, C. K. Kim, S. G. Youn, Y. S. Lee, M. Yoshio, and I. H. Oh, *Journal of Materials Chemistry*, **11**(10), 2519 (2001).
25. A. Antonini, C. Bellitto, M. Pasquali, and G. Pistoia, *Journal of the Electrochemical Society*, **145**(8), 2726 (1998).
26. Y. K. Sun, M. J. Lee, C. S. Yoon, J. Hassoun, K. Amine, and B. Scrosati, *Advanced Materials*, **24**(9), 1192 (2012).
27. J. S. Gnanaraj, V. G. Pol, A. Gedanken, and D. Aurbach, *Electrochemistry Communications*, **5**(11), 940 (2003).
28. S. Lim and J. Cho, *Electrochemistry Communications*, **10**(10), 1478 (2008).
29. I. H. Cho, S. S. Kim, S. C. Shin, and N. S. Choi, *Electrochemical and Solid State Letters*, **13**(11), A168 (2010).
30. P. Arora and Z. M. Zhang, *Chemical Reviews*, **104**(10), 4419 (2004).
31. J. M. Ko, B. G. Min, D. W. Kim, K. S. Ryu, K. M. Kim, Y. G. Lee, and S. H. Chang, *Electrochimica Acta*, **50**(2-3), 367 (2004).
32. Y. S. Jung, A. S. Cavanagh, L. Gedvilas, N. E. Widjonarko, I. D. Scott, S. H. Lee, G. H. Kim, S. M. George, and A. C. Dillon, *Advanced Energy Materials*, **2**(8), 1022 (2012).
33. J. D. Ferguson, A. W. Weimer, and S. M. George, *Chemistry of Materials*, **16**(26), 5602 (2004).
34. A. S. Huang, H. Bux, F. Steinbach, and J. Caro, *Angewandte Chemie-International Edition*, **49**(29), 4958 (2010).
35. Y. Park, D. S. Shin, S. H. Woo, N. S. Choi, K. H. Shin, S. M. Oh, K. T. Lee, and S. Y. Hong, *Advanced Materials*, **24**(26), 3562 (2012).